

# DICE: Distilling Classifier-Free Guidance into Text Embeddings

Zhenyu Zhou<sup>1</sup> Defang Chen<sup>2</sup> Can Wang<sup>1</sup> Chun Chen<sup>1</sup> Siwei Lyu<sup>2</sup>

## Abstract

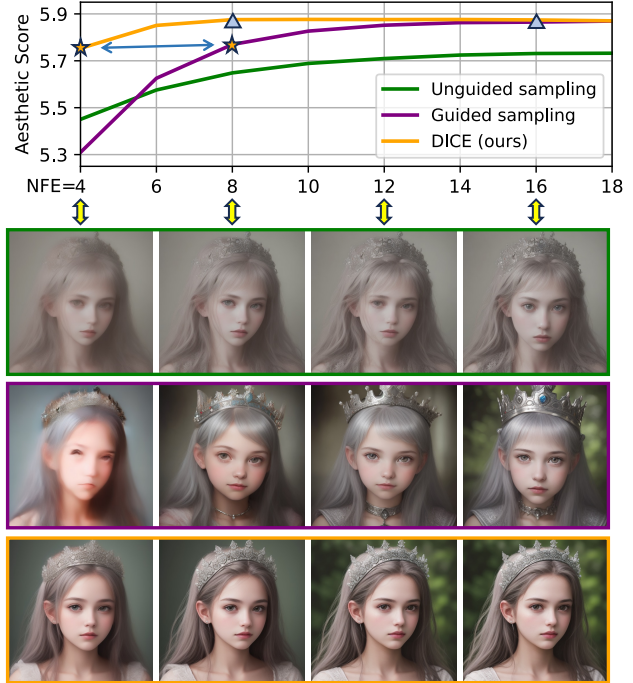
Text-to-image diffusion models are capable of generating high-quality images, but these images often fail to align closely with the given text prompts. Classifier-free guidance (CFG) is a popular and effective technique for improving text-image alignment in the generative process. However, using CFG introduces significant computational overhead and deviates from the established theoretical foundations of diffusion models. In this paper, we present **D**istilling **C**FG by enhancing text **E**mbeddings (DICE), a novel approach that removes the reliance on CFG in the generative process while maintaining the benefits it provides. DICE distills a CFG-based text-to-image diffusion model into a CFG-free version by refining text embeddings to replicate CFG-based directions. In this way, we avoid the computational and theoretical drawbacks of CFG, enabling high-quality, well-aligned image generation at a fast sampling speed. Extensive experiments on multiple Stable Diffusion v1.5 variants, SDXL and PixArt- $\alpha$  demonstrate the effectiveness of our method. Furthermore, DICE supports negative prompts for image editing to improve image quality further. Code will be available soon.

## 1. Introduction

Recently, diffusion models (Sohl-Dickstein et al., 2015; Song & Ermon, 2019; Ho et al., 2020) have achieved remarkable advances, driven by continuously refined theoretical frameworks (Song et al., 2021b; Karras et al., 2022; Chen et al., 2024a; Kingma & Gao, 2024) and fast evolution of effective model architectures (Peebles & Xie, 2023; Bao et al., 2023). Their impressive generation ability has brought text-to-image generation to unprecedented levels (Rombach et al., 2022; Saharia et al., 2022; Podell et al., 2024; Esser et al., 2024), and enables a multitude of new conditional generation tasks (Croitoru et al., 2023; Zhan et al., 2024).

<sup>1</sup>Zhejiang University <sup>2</sup>University at Buffalo. Correspondence to: Defang Chen <defangch@buffalo.edu>.

Preprint.



“Photo portrait of a girl in a silver crown.”

Figure 1: Comparison of Text-to-Image Generation: unguided sampling, guided sampling, and DICE. **Top:** Average aesthetic score (Schuhmann et al., 2022) over 5,000 generated images plotted against the number of function evaluations (NFE). **Bottom:** An example of image synthesis using different methods at NFE = 4, 8, 12, and 16. All images are generated by DreamShaper (Lykon, 2023) with the same random seed. Notably, compared to CFG-based sampling, DICE achieves comparable image quality with only half the NFE.

In text-to-image generation, diffusion models use text embeddings produced by pre-trained encoders such as CLIP (Radford et al., 2021) and T5 (Raffel et al., 2020) (Nichol et al., 2022; Rombach et al., 2022; Saharia et al., 2022), which are vectors encapsulating the semantic content in the text prompts. However, the text embeddings are not specifically tailored for image generation. Moreover, images often encompass more detailed information than text prompts can convey, making precise text-image semantic alignment challenging (Schrodi et al., 2024). Consequently, as illustrated in Figure 1, sampling with text-to-image models in the original conditional manner—referred to as *unguided sampling*—generally results in blurry, dis-

torted, and semantically inaccurate outputs (Meng et al., 2023; Karras et al., 2024). To address the limited semantic signals provided by text embeddings, *guided sampling* techniques (Dhariwal & Nichol, 2021; Ho & Salimans, 2022) have been introduced to steer samples toward a more concentrated distribution, enhancing image quality and alignment with the text prompts.

Classifier-Free Guidance (CFG) (Ho & Salimans, 2022) is a widely adopted technique for guided sampling. It directs the generative process at each sampling step by extrapolating the direction between the original conditional prediction and an unconditional prediction, with the guidance strength modulated by a hyperparameter known as the guidance scale. The application of CFG enhances the quality of the image and the alignment of the text with the image, establishing it as a practical and essential method. However, CFG requires an additional model evaluation at each step, thus increasing the sampling overhead (Ho & Salimans, 2022). Moreover, it disrupts the ability of diffusion models to capture the underlying data distribution, complicating the interpretation of sampling dynamics and causing a divergence from their well-established theoretical foundations (Karras et al., 2024; Zheng & Lan, 2024; Bradley & Nakkiran, 2024).

To mitigate the increased sampling overhead, prior research distilled CFG into a single model evaluation at each sampling step. These approaches either fine-tune all parameters of the text-to-image model (Meng et al., 2023; Li et al., 2024b) or train an auxiliary guided model (Hsiao et al., 2024). However, the theoretical issues associated with CFG in the distilled model remain unresolved.

In this paper, we introduce **D**Istilling CFG by enhancing text **E**mbeddings (DICE), a novel approach to achieving high-quality sample generation with unguided sampling by enhancing the model’s conditioning, specifically through optimized text embeddings (see Figure 2). These embeddings are refined under CFG-based supervision by training a lightweight enhancer that operates independently of the primary text-to-image model. With these optimized embeddings, our strengthened unguided sampling accelerates high-quality image generation, matching the performance of guided sampling. DICE maintains consistent theoretical foundations with traditional unguided sampling, offering improved interpretability in sampling dynamics. In addition, we show that DICE embeddings can be used across different base models. This is due to the property that DICE preserves essential semantic information while enhancing fine-grained details in the generated images. Extensive experiments across various text-to-image models, encompassing different model capacities, image styles, and network architectures, validate the effectiveness of our method in diverse scenarios. Furthermore, DICE supports negative prompts for image editing to improve image quality further.

## 2. Preliminaries

### 2.1. Diffusion Models and Text-to-image Generation

Given a data sample  $\mathbf{x}_0 \in \mathbb{R}^d$  from the implicit data distribution  $p_0$ , the forward process in diffusion models gradually adds white Gaussian noise to the sample, following a stochastic differential equation (SDE) (Song et al., 2021b):

$$d\mathbf{x}_t = \mathbf{f}(\mathbf{x}_t, t)dt + g(t)d\mathbf{w}_t, \quad t \in [0, T], \quad (1)$$

where  $\mathbf{f}(\cdot, t) : \mathbb{R}^d \rightarrow \mathbb{R}^d, g(\cdot) : \mathbb{R} \rightarrow \mathbb{R}$  are drift and diffusion coefficients and  $\mathbf{w}_t \in \mathbb{R}^d$  is the Wiener process (Ok-sendal, 2013). The backward process in diffusion models achieves the data reconstruction through a reverse-time SDE,  $d\mathbf{x}_t = [\mathbf{f}(\mathbf{x}_t, t) - g^2(t)\nabla_{\mathbf{x}_t} \log p_t(\mathbf{x}_t)]dt + g(t)d\bar{\mathbf{w}}_t$ , which shares the same marginal distributions  $\{p_t\}_{t=0}^T$  with the forward process (Song et al., 2021b). This reverse-time SDE has an ordinary differential equation (ODE) counterpart called *probability flow* ODE (PF-ODE) (Song et al., 2021b; Karras et al., 2022; Chen et al., 2024a), i.e.,  $d\mathbf{x}_t = [\mathbf{f}(\mathbf{x}_t, t) - \frac{1}{2}g^2(t)\nabla_{\mathbf{x}_t} \log p_t(\mathbf{x}_t)]dt$ . Following the parametrization in EDM (Karras et al., 2022), in this paper, we consider  $\mathbf{f}(\mathbf{x}_t, t) = \mathbf{0}$  and  $g(t) = \sqrt{2t}$  and simplify the PF-ODE into

$$d\mathbf{x}_t = -t\nabla_{\mathbf{x}_t} \log p_t(\mathbf{x}_t)dt. \quad (2)$$

The analytically intractable  $\nabla_{\mathbf{x}_t} \log p_t(\mathbf{x}_t)$  is known as the *score function* (Hyvärinen, 2005; Lyu, 2009), which is typically estimated by either a score-prediction model  $\mathbf{s}_\theta(\mathbf{x}_t)$ , or a noise-prediction model  $\epsilon_\theta(\mathbf{x}_t)$ , i.e.,

$$\nabla_{\mathbf{x}_t} \log p_t(\mathbf{x}_t) \approx \mathbf{s}_\theta(\mathbf{x}_t) = -\frac{\epsilon_\theta(\mathbf{x}_t)}{t}. \quad (3)$$

For simplicity, unless otherwise specified, we omit the time dependence on the model. Taking the noise-prediction model as an example, the training objective of diffusion models is the minimization of a regression loss with a weighting function  $\lambda(t)$  (Ho et al., 2020; Nichol & Dhariwal, 2021; Kingma & Gao, 2024):

$$\mathcal{L}(\theta) = \mathbb{E}_{t \sim \mathcal{U}(0, T), \epsilon \sim \mathcal{N}(\mathbf{0}, \mathbf{I})} [\lambda(t) \|\epsilon_\theta(\mathbf{x}_t) - \epsilon\|_2^2], \quad (4)$$

where  $\mathbf{x}_t = \mathbf{x}_0 + t\epsilon$ , and  $\mathbf{x}_0 \sim p_0$  follows the forward transition kernel  $p_{0t}(\mathbf{x}_t|\mathbf{x}_0) = \mathcal{N}(\mathbf{x}_t; \mathbf{x}_0, t^2\mathbf{I})$ .

In text-to-image generation, the diffusion model receives embeddings of a text prompt  $\mathbf{c} \in \mathbb{R}^{K \times d_e}$  encoded by a pre-trained text encoder to predict the score function conditioned on the text prompt, where  $K$  denotes the token number and  $d_e$  is the context dimension of each token. Starting from a random Gaussian noise  $\mathbf{x}_T$  with a manually designed time schedule, sampling from diffusion models is to numerically solve  $d\mathbf{x}_t = \epsilon_\theta(\mathbf{x}_t, \mathbf{c})dt$  through, for example, an Euler discretization (Song et al., 2021a),

$$\mathbf{x}_s = \mathbf{x}_t + (s - t) \epsilon_\theta(\mathbf{x}_t, \mathbf{c}), \quad (5)$$

where  $0 \leq s < t \leq T$ . Advanced numerical solvers can also be employed (Zhang & Chen, 2023; Zhou et al., 2024a).

## 2.2. Classifier-free Guidance

The standard class-conditional sampling for text-to-image generation with Equation (5) usually produces blurry, distorted, and semantically inaccurate images (Meng et al., 2023; Karras et al., 2024). In practice, classifier-free guidance (CFG) (Ho & Salimans, 2022) is widely used to trade sample fidelity with diversity, allowing the model to achieve low-temperature sampling without the need for an auxiliary classifier-based guidance (Dhariwal & Nichol, 2021). This technique modifies the model output by another model evaluation conditioned on a fixed null text embedding  $\mathbf{c}_{\text{null}}$

$$\epsilon_{\theta}^{\omega, \mathbf{c}_{\text{null}}}(\mathbf{x}_t, \mathbf{c}) = \omega \epsilon_{\theta}(\mathbf{x}_t, \mathbf{c}) - (\omega - 1) \epsilon_{\theta}(\mathbf{x}_t, \mathbf{c}_{\text{null}}), \quad (6)$$

$$\mathbf{x}_s = \mathbf{x}_t + (s - t) \epsilon_{\theta}^{\omega, \mathbf{c}_{\text{null}}}(\mathbf{x}_t, \mathbf{c}), \quad (7)$$

where  $\omega \geq 1$  is known as the *guidance scale*, with  $\omega = 1$  corresponding to unguided sampling, and  $\omega > 1$  to guided sampling. Despite the ability to perform high-quality generation, CFG requires one more model evaluation in each guided sampling step.

In unguided diffusion sampling, a key characteristic is that the forward and backward processes share identical marginal distributions, denoted as  $\{p_t(\mathbf{x}_t|\mathbf{c})\}_{t=0}^T$ . This symmetry allows us to know the exact distributions we sample from when solving Equation (2). However, this equivalence doesn't hold in guided sampling using Equation (6). While it might appear that samples adhere to a  $\omega$ -powered distribution  $p_{t,\omega}(\mathbf{x}_t|\mathbf{c}) \propto p_t^{\omega}(\mathbf{x}_t|\mathbf{c})p_t^{\omega-1}(\mathbf{x}_t)$ , they actually deviate from any known distributions produced by the forward diffusion process starting from  $p_{0,\omega}(\mathbf{x}_0|\mathbf{c})$  (Zheng & Lan, 2024)<sup>1</sup>. The CFG mechanism is believed to indiscriminately push samples toward regions the model deems favorable (Karras et al., 2024). The specific marginal distributions sampled by CFG remain an open question (Bradley & Nakkiran, 2024).

Previous works such as Guidance Distillation (Meng et al., 2023) and Plug-and-Play (Hsiao et al., 2024) have successfully distilled guided sampling into unguided ones. However, the theoretical issue remains in the distilled model, as they either directly modify the model parameters or inject an external model, disturbing the nature of diffusion models of predicting the ground-truth score function.

## 3. Method

Text-to-image diffusion models are trained on extensive datasets of text-image pairs (Rombach et al., 2022; Podell et al., 2024; Esser et al., 2024). In this process, text prompts

<sup>1</sup>In fact, it's unclear whether  $p_{t,\omega}(\mathbf{x}_t|\mathbf{c})$  constitutes a proper probability distribution, as it may not be integrable.

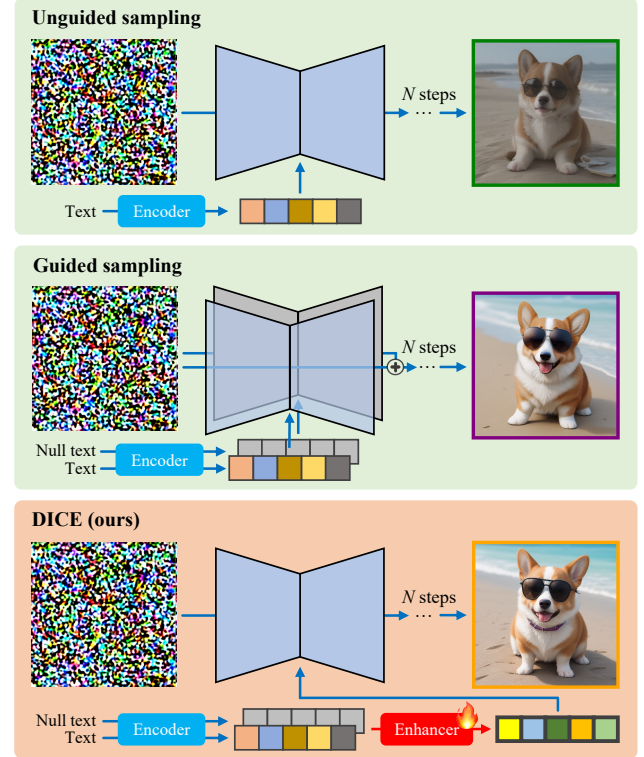


Figure 2: Overview of DICE sampling and comparison with traditional unguided and guided sampling. With enhanced text embeddings, DICE achieves high-quality image generation as the guided sampling while maintaining the same computational overhead of the unguided sampling.

are first encoded into embeddings using pre-trained text encoders (Radford et al., 2021; Raffel et al., 2020) and then integrated into the model’s inference through cross-attention modules. However, these models often struggle to generate images that closely align with the provided text prompts when using unguided sampling.

We hypothesize that this misalignment stems from two primary factors. First, there is an information imbalance between text and images. Images encapsulate rich details such as layout, texture, and fine-grained elements, whereas manually annotated captions typically describe only the main concepts (Radford et al., 2021; Schuhmann et al., 2022). This disparity leads to a well-known modality gap between texts and images (Liang et al., 2022; Schrodi et al., 2024). Second, given the vastness of the text prompt space, the dataset may lack prompts specifically designed by users.

Consequently, text embeddings from pre-trained text encoders generally lack sufficient information to fully describe images. Simultaneously, the text-to-image model is tasked with performing few-shot or even zero-shot generation, contributing to the challenges observed in unguided sampling.

Unguided sampling, while offering rapid execution and solid theoretical underpinnings, often yields subpar sample qual-

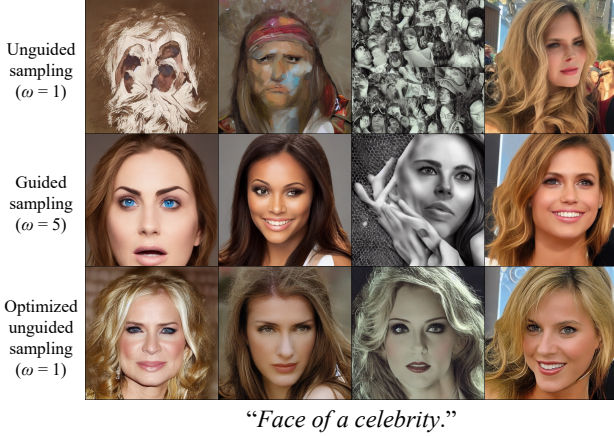


Figure 3: Images generated by Stable Diffusion v1.5 (Rombach et al., 2022) on the CelebA-HQ dataset (Karras, 2017) using 10-step DPM-Solver++ (Lu et al., 2022). Unguided sampling usually generates distorted or semantically inaccurate images. By fine-tuning a predefined text embedding, the optimized unguided sampling generates decent images on par with that obtained by the guided sampling. Images in the same column are generated with the same seed.

To enhance this, we aim to enrich each text embedding with more detailed information about its corresponding image. A straightforward approach is fine-tuning the embeddings of a specific text prompt. For instance, as shown in Figure 3, we achieve optimized unguided sampling that produces images comparable in quality to those generated through guided sampling. This preliminary study confirms the effectiveness of strengthening a single text prompt. However, fine-tuning on every possible text prompts is impractical and risks knowledge degradation.

### 3.1. Our Proposed DICE

We present **DI**stilling CFG by enhancing text **E**mbdings (DICE) that removes the reliance on CFG in the generative process while maintaining the benefits it provides. DICE distills a CFG-based text-to-image diffusion model into a CFG-free version by refining the text encoder to replicate the CFG-based direction. DICE avoids the computational and theoretical drawbacks of CFG and enables high-quality, well-aligned image generation at a fast sampling speed.

Specifically, given a text embedding  $\mathbf{c}$  encoded by the text encoder, we train a lightweight *enhancer*  $r_\phi(\cdot, \cdot) : \mathbb{R}^{(K \times d_e) \times (K \times d_e)} \rightarrow \mathbb{R}^{K \times d_e}$  with the trainable parameters  $\phi$ , to strengthen the original text embedding, i.e.,

$$\mathbf{c}_\phi = \mathbf{c} + \alpha r_\phi(\mathbf{c}, \mathbf{c}_{\text{null}}), \quad (8)$$

where  $\alpha$  is a hyperparameter controlling the strength. Similar to Equation (5), the unguided sampling becomes

$$\mathbf{x}_s = \mathbf{x}_t + (s - t) \epsilon_\theta(\mathbf{x}_t, \mathbf{c}_\phi). \quad (9)$$

We train the enhancer under CFG-based supervision and keep the model parameters  $\theta$  completely frozen. Given

### Algorithm 1 DICE Training

**Input:** dataset  $\mathcal{D}$ , guidance scale  $\omega$ , maximum timestamp  $T$ , text-to-image model  $\epsilon_\theta(\cdot, \cdot)$ , null text embedding  $\mathbf{c}_{\text{null}}$ , learning rate  $\eta$

**Initialize:** enhancer  $r_\phi(\cdot, \cdot)$

**while** not converged **do**

    Sample image-embedding pairs  $(\mathbf{x}_0, \mathbf{c}) \sim \mathcal{D}$

    Sample a timestamp  $t \sim \mathcal{U}(0, T)$

    Forward diffusion process  $\mathbf{x}_t \sim \mathcal{N}(\mathbf{x}_0, t^2 I)$

$\epsilon_\theta^{\omega, \mathbf{c}_{\text{null}}}(\mathbf{x}_t, \mathbf{c}) = \omega \epsilon_\theta(\mathbf{x}_t, \mathbf{c}) - (\omega - 1) \epsilon_\theta(\mathbf{x}_t, \mathbf{c}_{\text{null}})$

$\mathbf{c}_\phi = \mathbf{c} + \alpha r_\phi(\mathbf{c}, \mathbf{c}_{\text{null}})$

$\mathcal{L}(\phi) = \|\epsilon_\theta(\mathbf{x}_t, \mathbf{c}_\phi) - \epsilon_\theta^{\omega, \mathbf{c}_{\text{null}}}(\mathbf{x}_t, \mathbf{c})\|$

$\phi \leftarrow \phi - \eta \nabla_\phi \mathcal{L}(\phi)$

**end while**

image-embedding pairs  $(\mathbf{x}_0, \mathbf{c})$ , the training loss of the enhancer is designed in a distillation manner, as,

$$\mathbb{E}_{t \sim \mathcal{U}(0, T), \mathbf{x}_t \sim \mathcal{N}(\mathbf{x}_0, t^2 I)} \|\epsilon_\theta(\mathbf{x}_t, \mathbf{c}_\phi) - \epsilon_\theta^{\omega, \mathbf{c}_{\text{null}}}(\mathbf{x}_t, \mathbf{c})\|, \quad (10)$$

where the parameter to learn is  $\phi$  with  $\theta$  fixed. In experiments, we set the guidance scale  $\omega$  to 5. The detailed algorithm is shown in Algorithm 1.

Different from the most related works (Meng et al., 2023; Hsiao et al., 2024), which also reduce the sampling overhead brought by CFG, our method completely decouples the enhancer from the text-to-image model by only modifying the model condition, or specifically, text embeddings. Therefore, the text-to-image model still predicts the score function with respect to the implicit noised data distribution but conditioned on  $\mathbf{c}_\phi$ , i.e.,  $\nabla_{\mathbf{x}_t} \log p_t(\mathbf{x}_t | \mathbf{c}_\phi)$ . Consequently, the strengthened unguided sampling is grounded by the original theoretical foundations of diffusion models and generates samples from  $\{p_t(\mathbf{x}_t | \mathbf{c}_\phi)\}_{t=0}^T$  theoretically. A more detailed comparison to previous works is included in Appendix A.3.

### 3.2. Distilling Negative Prompts

In text-to-image generation, descriptive text prompts are typically termed as positive prompts. However, images generated solely from positive prompts may sometimes contain unnatural elements, such as extra limbs or unwanted objects, or may not meet the desired quality standards. To address these issues, negative prompts are employed for image editing and quality enhancement.

Given an embedding of a negative prompt (e.g., “bad quality”) denoted as  $\mathbf{c}_n$ , it replaces the null text embedding in the classifier-free guidance (CFG) equation:

$$\epsilon_\theta^{\omega, \mathbf{c}_n}(\mathbf{x}_t, \mathbf{c}) = \omega \epsilon_\theta(\mathbf{x}_t, \mathbf{c}) - (\omega - 1) \epsilon_\theta(\mathbf{x}_t, \mathbf{c}_n). \quad (11)$$

Previous works that distill the guidance scale omit the entry for negative prompts, limiting practical applicability.

Conversely, retaining the negative prompt in Equation 11 perpetuates the same issues inherent in CFG. To overcome this, we integrate the embedding of negative text prompts into the enhancer and strengthen the original embedding by  $\mathbf{c}_\phi = \mathbf{c} + \alpha r_\phi(\mathbf{c}, \mathbf{c}_n)$ . During training, negative prompts are randomly sampled from open-source datasets, and the training process remains consistent with Algorithm 1, except that negative text embeddings replace all null text embeddings.

## 4. Experiments

### 4.1. Settings

**Models and datasets.** Our experiments are conducted on Stable Diffusion v1.5 (SD15) (Rombach et al., 2022), Stable Diffusion XL (SDXL) (Podell et al., 2024), Pixart- $\alpha$  (Chen et al., 2024b) and a series of SD15-based open source variants, including DreamShaper<sup>2</sup>, AbsoluteReality<sup>3</sup>, Anime Pastel Dream<sup>4</sup>, DreamShaper PixelArt<sup>5</sup>, and 3D Animation Diffusion<sup>6</sup>. A detailed model summary is provided in Appendix A.1. We use MS-COCO 2017 (Lin et al., 2014) for training and evaluation.

**Training.** The lightweight enhancer consists of two fully-connected layers and an attention block. The number of trainable parameters is negligible compared to that of the text-to-image model (less than 1%), resulting in negligible increased computational overhead. The strength  $\alpha = 1$  and guidance scale  $\omega = 5$  are fixed for all experiments. For optimization, we use Adam optimizer (Kingma & Ba, 2014) with  $\beta_1 = 0.9$ ,  $\beta_2 = 0.999$ , learning rate of  $2e-4$  and batch size of 128. Enhancers for SD15-based variants are trained with negative prompts. All enhancers are trained with around 8,000 gradient updates, requiring 4.5, 6, 18 hours for SD15-based variants, Pixart- $\alpha$  and Stable Diffusion XL, respectively, using 8 NVIDIA A100 GPUs.

**Evaluation.** The sample quality is evaluated by Fréchet Inception Distance (FID) (Heusel et al., 2017), CLIP Score (CS) (Radford et al., 2021) and Aesthetic Score (AS) (Schuhmann et al., 2022). To compute FID, we generate 5K images using 5K prompts sampled from MS-COCO 2017 validation set and use the validation set as reference images. The generated 5K images are also used to compute CS and AS.

<sup>2</sup><https://huggingface.co/Lykon/DreamShaper>

<sup>3</sup>[https://huggingface.co/digisplay/AbsoluteReality\\_v1.8.1](https://huggingface.co/digisplay/AbsoluteReality_v1.8.1)

<sup>4</sup><https://huggingface.co/Lykon/AnimePastelDream>

<sup>5</sup><https://civitai.com/models/129879/dreamshaper-pixelart>

<sup>6</sup><https://civitai.com/models/118086?modelVersionId=128046>

Table 1: Quantitative results evaluated by Fréchet Inception Distance (FID), CLIP Score (CS) and Aesthetic Score (AS). Images are generated with the same random seeds by 20-step DPM-Solver++ (Lu et al., 2022). NFE denotes the number of function evaluations. GD denotes Guided Distillation (Meng et al., 2023), which is reimplemented with the same training iterations as our method.

Model	$\omega$	FID ( $\downarrow$ )	CS ( $\uparrow$ )	AS ( $\uparrow$ )	NFE
SD15	1	32.80	21.99	5.03	20
SD15	5	<b>22.04</b>	<b>30.22</b>	<b>5.36</b>	40
+ GD	5	26.63	29.22	5.30	20
+ DICE	1	22.22	28.54	5.28	20
DreamShaper	1	<b>24.17</b>	27.22	5.74	20
DreamShaper	5	30.35	<b>30.50</b>	<b>5.87</b>	40
+ GD	5	36.24	29.66	5.72	20
+ DICE	1	30.36	29.03	<b>5.87</b>	20
SDXL	1	61.19	21.92	5.59	20
SDXL	5	<b>23.95</b>	<b>32.10</b>	5.60	40
+ DICE	1	28.01	30.63	<b>5.68</b>	20
Pixart- $\alpha$	1	41.74	25.30	<b>6.11</b>	20
Pixart- $\alpha$	5	<b>38.39</b>	<b>30.67</b>	6.03	40
+ DICE	1	39.80	29.51	6.01	20

### 4.2. Text-to-Image Generation

We evaluate DICE on text-to-image models of varying capacities, with the number of parameters ranging from 0.6B to 2.6B, architectures such as U-Net (Ronneberger et al., 2015) and DiT (Peebles & Xie, 2023), and image styles including the dream, realistic, 3-D, pixel, and anime style. The quantitative results are presented in Table 1. Our strengthened unguided sampling achieves a sample quality comparable to that of guided sampling and largely outperforms the original unguided sampling with qualitative results shown in Figure 4. Moreover, with only text embedding modified, DICE achieves comparable results with Guidance Distillation (Meng et al., 2023), which fine-tunes the whole text-to-image model.

**Sampling budget.** In Figure 5, we report the performance of our method and guided sampling evolving with the number of function evaluations (NFE). As CFG requires an additional model evaluation (Equation (6)), the NFE for every single guided sampling step is 2 and otherwise 1. Our method demonstrates superiority over guided sampling when operating under a low NFE budget. Besides, the sample quality of our method exhibits an early convergence, which can be attributed to the smoother sampling trajectories (Chen et al., 2024a) generated by unguided sampling, as revealed in (Zhou et al., 2024b). More qualitative results are shown in Appendix A.5.

**Generalization.** As the enhancer operates independently of the text-to-image model, we investigate the feasibility of applying a well-trained enhancer to unseen text-to-image

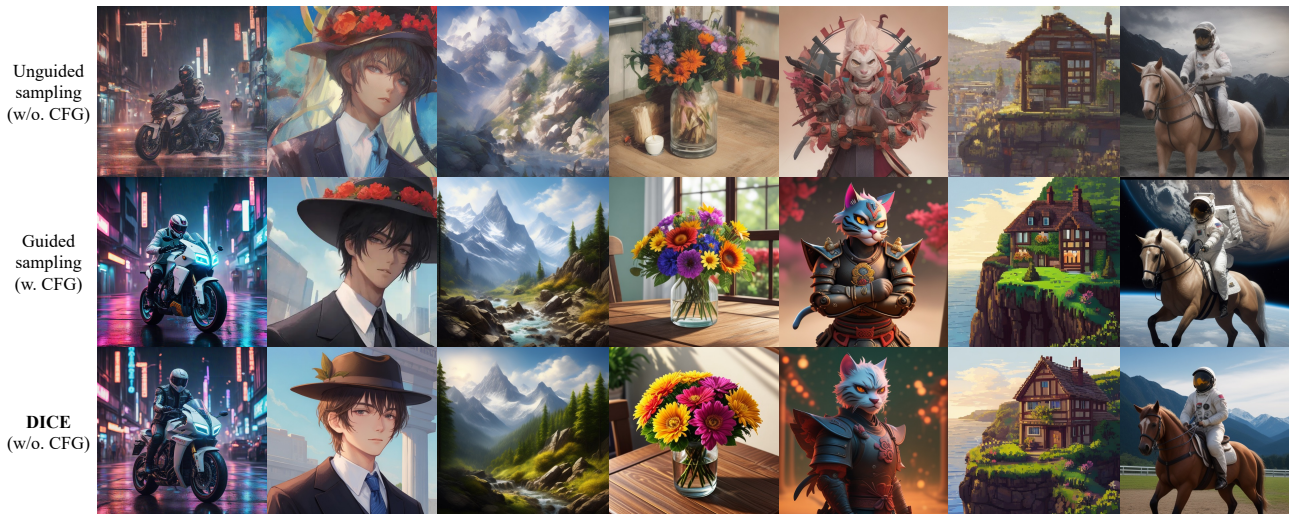


Figure 4: Qualitative results on text-to-image models with different model capacities, image styles and network architectures. Images are generated by 20-step DPM-Solver++ (Lu et al., 2022) on 7 text-to-image models including multiple Stable Diffusion v1.5 variants (Rombach et al., 2022), SDXL (Podell et al., 2024) and Pixart- $\alpha$  (Chen et al., 2024b). The used prompts are provided in Appendix A.1.

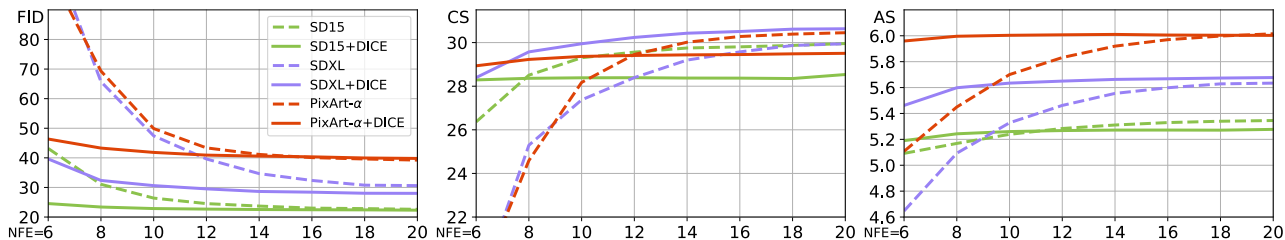


Figure 5: The comparison of FID (left), CLIP Score (middle), and Aesthetic Score (right) with respect to different numbers of function evaluations (NFE). Our proposed DICE converges faster than the guided sampling based on CFG.

models. We separately train three enhancers (enhancer  $i$ ,  $i = 1, 2, 3$ ) on three distinct text-to-image models, i.e., DreamShaper (model 1), DreamShaper PixelArt (model 2) and Anime Pastel Dream (model 3). Subsequently, we plug each enhancer into all of the models for unguided image generation. The results in Figure 6 shows that the enhancers exhibit strong generalization capabilities across diverse domains, consistently and significantly improving the original unguided sampling.

### 4.3. Understanding the Enhanced Text Embedding

We next explore the underlying mechanism of our method and show how the enhanced text embeddings impact the sample quality and sampling dynamics through both quantitative and qualitative evidence.

The text embedding used for text-to-image generation consists of a  $\langle SOS \rangle$  token, some semantic tokens and the remaining padded  $\langle EOS \rangle$  tokens. As revealed by previous works, e.g., (Yu et al., 2024), based on the position of the first  $\langle EOS \rangle$  token, a text embedding can be divided into

a semantic embedding that contains most semantic information and a padding embedding that encodes more about the image details. To verify this, in Figure 7, we replace the original embedding with enhanced semantic and padding embeddings. To replace the padding embedding, we can first recognize the index of the first  $\langle EOS \rangle$  token. Then, replace the embedding after this token with an enhanced one. We compute the cosine similarity between 1,000 paired original and enhanced semantic embeddings, obtaining a mean value of 0.75 and standard deviation of 0.05, while for padding embeddings, they are 0.23 and 0.02. This indicates that DICE emphasizes enhancing the padding embedding while mainly maintaining the original semantic embedding, leading to consistent semantic information but significantly improved image details.



Figure 6: Generalization of DICE text enhancer across different base models. Text enhancer  $i = 1, 2, 3$  is independently trained on model DreamShaper (model 1), DreamShaper PixelArt (model 2) and Anime Pastel Dream (model 3), and applied to other base models. The DICE enhancers lead to better image qualities than the unguided sampling without strengthening text embedding.



Figure 8: Effect of the text enhancer strength  $\alpha$ . As  $\alpha$  increases, the enhancer can maintain the semantic information while improving the sample quality. Images are generated by DreamShaper.

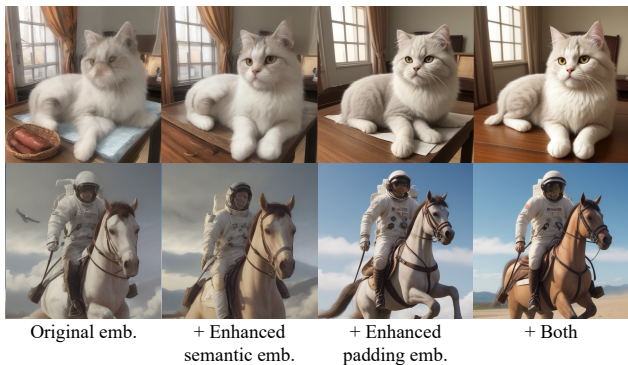


Figure 7: Replacing the original text embedding with the enhanced semantic and padding embedding. The enhanced padding embedding largely improves the sample quality. Images are generated by DreamShaper with text prompts “a cute Persian cat sitting on the table” (top) and “photo of an astronaut riding a horse”.

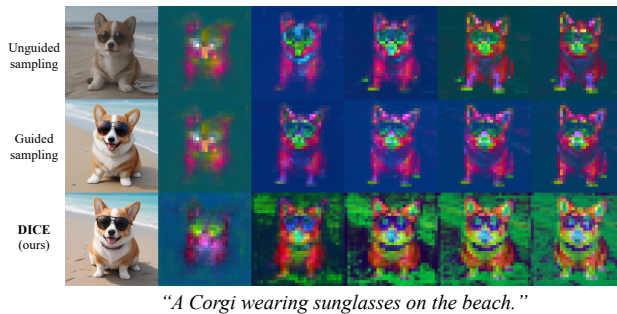


Figure 9: Visualization of cross-attention maps as sampling progresses. While all models can reproduce the main concepts, DICE emphasizes refining the image details.

Serving as both further evidence and an ablation study, we examine the effect of the enhancer strength  $\alpha$ , which is fixed to 1 during training and  $\alpha = 0$  corresponds to the original unguided sampling. As shown in Figure 8 (with more quantitative results included in Appendix A.5), with the increase of  $\alpha$ , the generated image improves with richer details and stronger contrast while preserving consistent semantic information. These results demonstrate that the enhancer manages to find semantically robust directions that steadily improve the image details.

In Figure 9, we further visualize the cross-attention maps of the U-Net decoder with the  $32 \times 32$  resolution to show the changes in the sampling dynamics. While the main concepts are activated in all the cases, the enhanced embedding further activates the image details, which can be seen from the constantly changing background of the attention maps. This also aligns with our conclusion of the mechanism of DICE down above. See Appendix A.5 for more results.

#### 4.4. Negative Prompts

As shown in Section 3.2, DICE sampling retains the capability of using negative prompts. In Figure 10, we show the effectiveness of DICE on the two main purposes of using negative prompts. Our method can perform desirable image editing and quality improvement, including modifying unnatural limbs, removing or changing unwanted features, and handling abstract prompts related to image quality.

### 5. Related Works

To the best of our knowledge, no existing work has explored the distillation approach to remove classifier-free guidance (CFG). However, recent studies have investigated alternative methods to enhance the efficiency of CFG-based generators.

**Understanding CFG.** Guided sampling in diffusion models was initially achieved through classifier guidance (Dhariwal & Nichol, 2021), utilizing an auxiliary classifier trained on noisy data. Classifier-free guidance (CFG)(Ho & Salimans, 2022) offers a streamlined approach to guided sampling

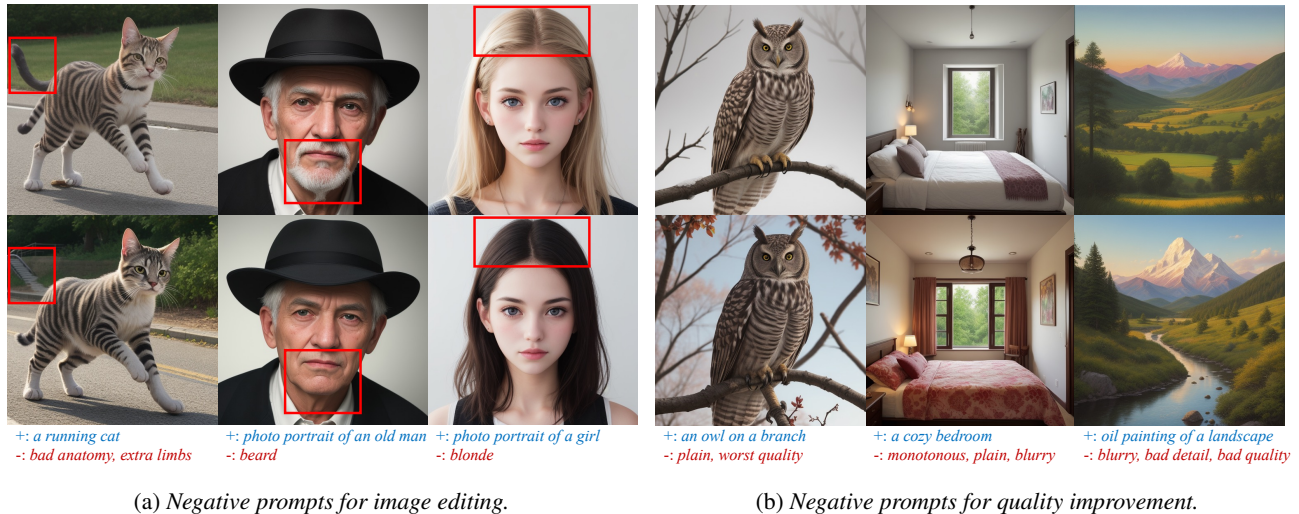


Figure 10: Performance of DICE on negative prompts. Positive and negative prompts are denoted by + and -.

without the need for a separately trained classifier and has become a fundamental technique in text-to-image generation (Rombach et al., 2022). Recent efforts have aimed to elucidate its mechanism. For instance, Characteristic Guidance (Zheng & Lan, 2024) reveals that the score function in CFG does not adhere to the Fokker-Planck equation (Lai et al., 2023), and CFG is considered to blindly push samples in a model-preferred direction (Karras et al., 2024). Additionally, a CFG step in stochastic sampling can be decomposed into a deterministic unguided step followed by a Langevin dynamics step (Bradley & Nakkiran, 2024). To date, the underlying behavior of CFG remains an area requiring further exploration.

**CFG distillation.** Previous works have proposed distilling CFG-based text-to-image models. Guided distillation (Meng et al., 2023) incorporates the guidance scale as a new model input through fine-tuning, a method later adopted by SnapFusion (Li et al., 2024b) and FLUX<sup>7</sup>. Plug-and-Play (Hsiao et al., 2024) trains an auxiliary guided model attached to the U-Net decoder, which is transferable to new domains. In contrast, our method solely modifies the text conditioning without altering the generative process of diffusion models. A more detailed comparison is provided in Appendix A.3.

**Reward-based methods.** The text encoder plays a crucial role in text-to-image generation. Several studies aim to improve guided sampling by fine-tuning the text encoder through reinforcement learning (Chen et al., 2025) and reward propagation (Li et al., 2024a). Our method differs in three key aspects. First, it is specifically designed to improve unguided sampling without relying on CFG. Second, it is trained under CFG-based supervision and does not require

human feedback or any reward models. Finally, as demonstrated in Appendix A.4, the text embeddings obtained by these methods are unsuitable for unguided sampling, highlighting the superiority of our method’s distinct mechanism.

## 6. Conclusion

Classifier-Free Guidance (CFG) is a prevalent technique in text-to-image generation, enhancing image quality but introducing increased sampling overhead and theoretical inconsistencies. In this work, we introduce DICE, which fortifies text embeddings by training an enhancer under CFG-based supervision. This approach achieves efficient and effective unguided text-to-image generation while maintaining theoretical consistency with the original unguided sampling. Qualitative and quantitative analyses reveal that DICE enhances fine-grained image details without compromising essential semantic information. Extensive experiments across various model capacities, image styles, and architectures demonstrate the effectiveness and robustness of our method. Our approach also supports the use of negative prompts for image editing and quality improvement, and it exhibits the capability to transfer to new domains.

**Limitations and future work.** Our method is trained under CFG, which may constrain its performance during guided sampling. To overcome this limitation, future work will focus on enhancing our method beyond guided sampling. Additionally, projecting the enhanced embeddings back to prompts could lead to a training-free approach by specifying potential trigger prompts. Exploring ways to improve unguided sampling without CFG-based supervision is also a promising direction.

<sup>7</sup><https://github.com/black-forest-labs/flux>

## Impact Statement

Similar to existing works on text-to-image generation, our method have the potential to be abused for generating malicious images that could be indistinguishable from real ones, raising concerns about harmful social impacts. This risk can be mitigated through advanced deep forgery detection as well as model watermark techniques. By improving these detection and watermarking methods, we can help ensure the responsible and ethical use of text-to-image generation.

## References

- Bao, F., Nie, S., Xue, K., Cao, Y., Li, C., Su, H., and Zhu, J. All are worth words: A vit backbone for diffusion models. In *Proceedings of the IEEE/CVF conference on computer vision and pattern recognition*, pp. 22669–22679, 2023.
- Bradley, A. and Nakkiran, P. Classifier-free guidance is a predictor-corrector. *arXiv preprint arXiv:2408.09000*, 2024.
- Chen, C., Wang, A., Wu, H., Liao, L., Sun, W., Yan, Q., and Lin, W. Enhancing diffusion models with text-encoder reinforcement learning. In *European Conference on Computer Vision*, pp. 182–198. Springer, 2025.
- Chen, D., Zhou, Z., Wang, C., Shen, C., and Lyu, S. On the trajectory regularity of ODE-based diffusion sampling. In *International Conference on Machine Learning*, pp. 7905–7934. PMLR, 2024a.
- Chen, J., Yu, J., Ge, C., Yao, L., Xie, E., Wu, Y., Wang, Z., Kwok, J., Luo, P., Lu, H., et al. Pixart- $\alpha$ : Fast training of diffusion transformer for photorealistic text-to-image synthesis. In *International Conference on Learning Representations*, 2024b.
- Croitoru, F.-A., Hondru, V., Ionescu, R. T., and Shah, M. Diffusion models in vision: A survey. *IEEE Transactions on Pattern Analysis and Machine Intelligence*, 45(9):10850–10869, 2023.
- Dhariwal, P. and Nichol, A. Diffusion models beat gans on image synthesis. In *Advances in Neural Information Processing Systems*, 2021.
- Esser, P., Kulal, S., Blattmann, A., Entezari, R., Müller, J., Saini, H., Levi, Y., Lorenz, D., Sauer, A., Boesel, F., et al. Scaling rectified flow transformers for high-resolution image synthesis. In *Forty-first International Conference on Machine Learning*, 2024.
- Heusel, M., Ramsauer, H., Unterthiner, T., Nessler, B., and Hochreiter, S. GANs trained by a two time-scale update rule converge to a local Nash equilibrium. In *Advances in Neural Information Processing Systems*, pp. 6626–6637, 2017.
- Ho, J. and Salimans, T. Classifier-free diffusion guidance. *arXiv preprint arXiv:2207.12598*, 2022.
- Ho, J., Jain, A., and Abbeel, P. Denoising diffusion probabilistic models. In *Advances in Neural Information Processing Systems*, 2020.
- Hsiao, Y.-T., Khodadadeh, S., Duarte, K., Lin, W.-A., Qu, H., Kwon, M., and Kalarot, R. Plug-and-play diffusion distillation. In *Proceedings of the IEEE/CVF Conference on Computer Vision and Pattern Recognition*, pp. 13743–13752, 2024.
- Hyvärinen, A. Estimation of non-normalized statistical models by score matching. *Journal of Machine Learning Research*, 6:695–709, 2005.
- Karras, T. Progressive growing of gans for improved quality, stability, and variation. *arXiv preprint arXiv:1710.10196*, 2017.
- Karras, T., Aittala, M., Aila, T., and Laine, S. Elucidating the design space of diffusion-based generative models. In *Advances in Neural Information Processing Systems*, 2022.
- Karras, T., Aittala, M., Kynkäänniemi, T., Lehtinen, J., Aila, T., and Laine, S. Guiding a diffusion model with a bad version of itself. *arXiv preprint arXiv:2406.02507*, 2024.
- Kingma, D. and Gao, R. Understanding diffusion objectives as the elbo with simple data augmentation. *Advances in Neural Information Processing Systems*, 36, 2024.
- Kingma, D. P. and Ba, J. Adam: A method for stochastic optimization. *arXiv preprint arXiv:1412.6980*, 2014.
- Lai, C.-H., Takida, Y., Murata, N., Uesaka, T., Mitsufuji, Y., and Ermon, S. Fp-diffusion: Improving score-based diffusion models by enforcing the underlying score fokker-planck equation. In *International Conference on Machine Learning*, pp. 18365–18398. PMLR, 2023.
- Li, Y., Liu, X., Kag, A., Hu, J., Idelbayev, Y., Sagar, D., Wang, Y., Tulyakov, S., and Ren, J. Textcrafter: Your text encoder can be image quality controller. In *Proceedings of the IEEE/CVF Conference on Computer Vision and Pattern Recognition*, pp. 7985–7995, 2024a.
- Li, Y., Wang, H., Jin, Q., Hu, J., Chemerys, P., Fu, Y., Wang, Y., Tulyakov, S., and Ren, J. Snapfusion: Text-to-image diffusion model on mobile devices within two seconds. *Advances in Neural Information Processing Systems*, 36, 2024b.
- Liang, V. W., Zhang, Y., Kwon, Y., Yeung, S., and Zou, J. Y. Mind the gap: Understanding the modality gap in multi-modal contrastive representation learning. *Advances in Neural Information Processing Systems*, 35: 17612–17625, 2022.

- Lin, T.-Y., Maire, M., Belongie, S., Hays, J., Perona, P., Ramanan, D., Dollár, P., and Zitnick, C. L. Microsoft coco: Common objects in context. In *Computer Vision–ECCV 2014: 13th European Conference, Zurich, Switzerland, September 6–12, 2014, Proceedings, Part V 13*, pp. 740–755. Springer, 2014.
- Lu, C., Zhou, Y., Bao, F., Chen, J., Li, C., and Zhu, J. Dpm-solver++: Fast solver for guided sampling of diffusion probabilistic models. *arXiv preprint arXiv:2211.01095*, 2022.
- Lykon. Dreamshaper. <https://huggingface.co/Lykon/DreamShaper>, 2023.
- Lyu, S. Interpretation and generalization of score matching. In *Proceedings of the Twenty-Fifth Conference on Uncertainty in Artificial Intelligence*, pp. 359–366, 2009.
- Meng, C., Rombach, R., Gao, R., Kingma, D., Ermon, S., Ho, J., and Salimans, T. On distillation of guided diffusion models. In *Proceedings of the IEEE/CVF Conference on Computer Vision and Pattern Recognition*, pp. 14297–14306, 2023.
- Nichol, A. Q. and Dhariwal, P. Improved denoising diffusion probabilistic models. In *International Conference on Machine Learning*, pp. 8162–8171. PMLR, 2021.
- Nichol, A. Q., Dhariwal, P., Ramesh, A., Shyam, P., Mishkin, P., Mcgrew, B., Sutskever, I., and Chen, M. Glide: Towards photorealistic image generation and editing with text-guided diffusion models. In *International Conference on Machine Learning*, pp. 16784–16804. PMLR, 2022.
- Oksendal, B. *Stochastic differential equations: an introduction with applications*. Springer Science & Business Media, 2013.
- Peebles, W. and Xie, S. Scalable diffusion models with transformers. In *Proceedings of the IEEE/CVF International Conference on Computer Vision*, pp. 4195–4205, 2023.
- Podell, D., English, Z., Lacey, K., Blattmann, A., Dockhorn, T., Müller, J., Penna, J., and Rombach, R. Sdxl: Improving latent diffusion models for high-resolution image synthesis. In *International Conference on Learning Representations*, 2024.
- Radford, A., Kim, J. W., Hallacy, C., Ramesh, A., Goh, G., Agarwal, S., Sastry, G., Askell, A., Mishkin, P., Clark, J., et al. Learning transferable visual models from natural language supervision. In *International conference on machine learning*, pp. 8748–8763. PMLR, 2021.
- Raffel, C., Shazeer, N., Roberts, A., Lee, K., Narang, S., Matena, M., Zhou, Y., Li, W., and Liu, P. J. Exploring the limits of transfer learning with a unified text-to-text transformer. *Journal of machine learning research*, 21 (140):1–67, 2020.
- Rombach, R., Blattmann, A., Lorenz, D., Esser, P., and Ommer, B. High-resolution image synthesis with latent diffusion models. In *Proceedings of the IEEE/CVF Conference on Computer Vision and Pattern Recognition*, pp. 10684–10695, 2022.
- Ronneberger, O., Fischer, P., and Brox, T. U-net: Convolutional networks for biomedical image segmentation. In *Medical Image Computing and Computer-Assisted Intervention–MICCAI 2015: 18th International Conference, Munich, Germany, October 5–9, 2015, Proceedings, Part III 18*, pp. 234–241. Springer, 2015.
- Saharia, C., Chan, W., Saxena, S., Li, L., Whang, J., Denton, E. L., Ghasemipour, K., Gontijo Lopes, R., Karagol Ayan, B., Salimans, T., et al. Photorealistic text-to-image diffusion models with deep language understanding. In *Advances in Neural Information Processing Systems*, pp. 36479–36494, 2022.
- Schrodi, S., Hoffmann, D. T., Argus, M., Fischer, V., and Brox, T. Two effects, one trigger: On the modality gap, object bias, and information imbalance in contrastive vision-language representation learning. *arXiv preprint arXiv:2404.07983*, 2024.
- Schuhmann, C., Beaumont, R., Vencu, R., Gordon, C., Wightman, R., Cherti, M., Coombes, T., Katta, A., Mullis, C., Wortsman, M., et al. Laion-5b: An open large-scale dataset for training next generation image-text models. *Advances in Neural Information Processing Systems*, 35: 25278–25294, 2022.
- Sohl-Dickstein, J., Weiss, E., Maheswaranathan, N., and Ganguli, S. Deep unsupervised learning using nonequilibrium thermodynamics. In *International conference on machine learning*, pp. 2256–2265. PMLR, 2015.
- Song, J., Meng, C., and Ermon, S. Denoising diffusion implicit models. In *International Conference on Learning Representations*, 2021a.
- Song, Y. and Ermon, S. Generative modeling by estimating gradients of the data distribution. In *Advances in Neural Information Processing Systems*, 2019.
- Song, Y., Sohl-Dickstein, J., Kingma, D. P., Kumar, A., Ermon, S., and Poole, B. Score-based generative modeling through stochastic differential equations. In *International Conference on Learning Representations*, 2021b.

- Yu, H., Luo, H., Wang, F., and Zhao, F. Uncovering the text embedding in text-to-image diffusion models. *arXiv preprint arXiv:2404.01154*, 2024.
- Zhan, Z., Chen, D., Mei, J.-P., Zhao, Z., Chen, J., Chen, C., Lyu, S., and Wang, C. Conditional image synthesis with diffusion models: A survey. *arXiv preprint arXiv:2409.19365*, 2024.
- Zhang, L., Rao, A., and Agrawala, M. Adding conditional control to text-to-image diffusion models. In *Proceedings of the IEEE/CVF International Conference on Computer Vision*, pp. 3836–3847, 2023.
- Zhang, Q. and Chen, Y. Fast sampling of diffusion models with exponential integrator. In *International Conference on Learning Representations*, 2023.
- Zheng, C. and Lan, Y. Characteristic guidance: Non-linear correction for diffusion model at large guidance scale. In *Forty-first International Conference on Machine Learning*, 2024.
- Zhou, Z., Chen, D., Wang, C., and Chen, C. Fast ode-based sampling for diffusion models in around 5 steps. In *Proceedings of the IEEE/CVF Conference on Computer Vision and Pattern Recognition*, pp. 4401–4410, 2024a.
- Zhou, Z., Chen, D., Wang, C., Chen, C., and Lyu, S. Simple and fast distillation of diffusion models. *arXiv preprint arXiv:2409.19681*, 2024b.

Table 2: Text-to-image models and text prompts used in Figure 4.

Model	Text prompt
SDXL (Podell et al., 2024)	<i>A rainy street, a racer on a white motorcycle by the street, bright neon lights, cyberpunk style, futuristic, 8k, best quality, clear background</i>
Anime Pastel Dream Pixart- $\alpha$ (Chen et al., 2024b)	<i>A man in suits and hat, center, close-up, best quality</i>
AbsoluteReality	<i>Epic scene, mountains, sunshine, trees, rocks, clear, realistic, best quality, best detail, aesthetic, masterpiece</i>
3D Animation Diffusion	<i>Colorful flowers in a vase on a wooden table, sunshine, aesthetic, realistic, 8k, best quality</i>
DreamShaper PixelArt DreamShaper	<i>An anthropomorphic cat samurai wearing armor, bokeh temple background, colorful, masterpieces, best quality, aesthetic</i> <i>A countryside cottage on the edge of a cliff overlooking an ocean, pixel art</i> <i>Photo of an astronaut riding a horse</i>

Table 3: Summary of used text-to-image models.

Model	SD15 variants	SDXL	PixArt- $\alpha$
Model architecture	U-Net	U-Net	DiT
# of model parameters	0.86B	2.58B	0.61B
Text encoder	CLIP ViT-L	CLIP ViT-L & OpenCLIP ViT-bigG	Flan-T5-XXL
# of tokens	77	77	120
Context dimension	768	2048	4096
# of encoder parameters	0.12B	0.82B	4.76B
# of enhancer parameters	1.84M	3.15M	5.25M

## A. Appendix

### A.1. Additional Details

The text prompts and models used to generate Figure 4 are listed in Table 2. They are selected to generate images with as many image styles and topics as possible.

In Table 3, we summarize all the text-to-image models used in our experiments. SD15 variants (Rombach et al., 2022) and SDXL (Podell et al., 2024) use U-Net (Ronneberger et al., 2015) as backbone while PixArt- $\alpha$  (Chen et al., 2024b) uses DiT (Peebles & Xie, 2023). Different pre-trained text encoders are used for each type of text-to-image model with the number of parameters ranging from different orders of magnitude.

For the enhancer, we use two fully-connected layers and one cross-attention layer. The first fully-connected layer compresses the input two text embeddings into a context dimension of 512. The obtained two features are then input to the cross-attention layer and are finally extended to the original context dimension through the second fully-connected layer. The number of parameters of the obtained enhancer account for 0.21%, 0.12% and 0.86% of SD15 variants, SDXL and PixArt- $\alpha$ , respectively. The extra sampling overhead of the enhancer is negligible since it only runs once for every generation. Additionally, we find that the performance of the enhancer is insensitive to model structure. The inner context dimension of 512 is set with the aim of reducing the number of parameters of the enhancer.

### A.2. Visualizing the Enhanced Text Embeddings

We visualize 1,000 text embeddings with dimension of 59,136 ( $77 \times 768$ ) through standard principle component analysis (PCA). The results are shown in Figure 11, where the blue and red scatters denotes the original and enhanced text embeddings respectively. Remarkably, the enhanced text embeddings are distributed on a low-dimensional manifold with 34% of variance explained by the top 3 PCs, while for the original embeddings it is 8%. For enhanced text embedding, 60 principle components (PCs) are required to reach a PCA ratio of 80% and for the original text embedding it is around 300. Therefore, our enhancer locates a low-dimensional manifold in the vast ambient space which consists of around 60K dimensions.

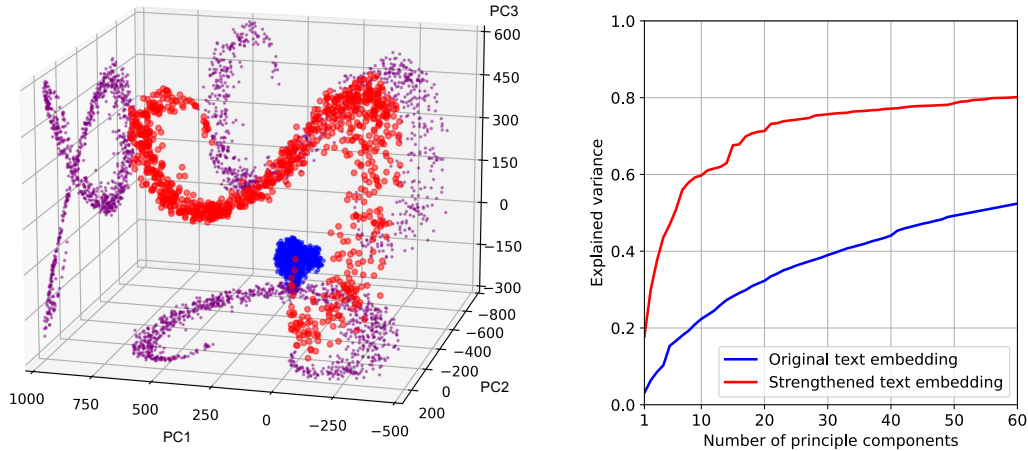


Figure 11: Left: visualization of 1,000 text embeddings through standard PCA. Blue scatters are the original text embeddings. The enhanced embeddings (red scatters) are distributed on a low-dimensional manifold. Purple scatters are the projection of red scatters on 2-D planes. Right: explained variance v.s. the number of principle components.

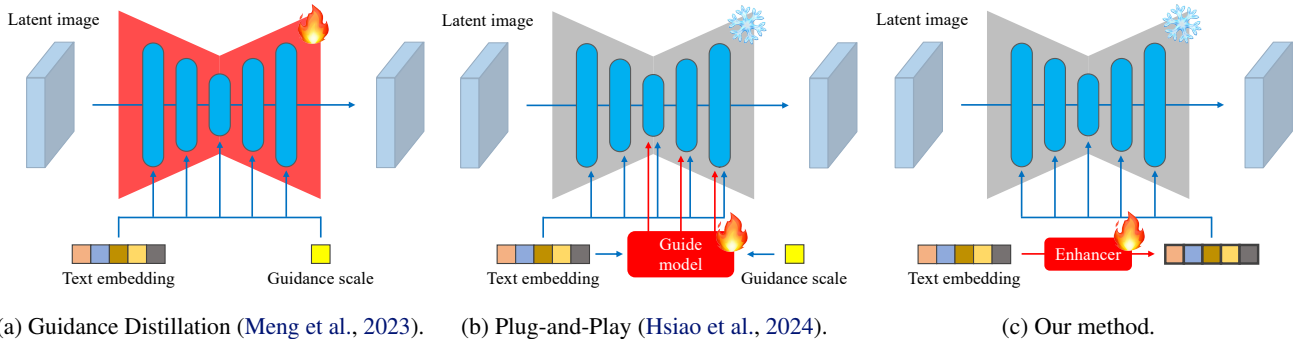


Figure 12: Method comparison. (a) Guidance Distillation takes guidance scale as an additional entry and fine-tune the whole text-to-image model. The way to process the guidance scale is similar to that of the timestamp. (b) Plug-and-Play takes inspiration from ControlNet and trains an external guide model to distill the guidance scale. (c) Our method trains an enhancer to strengthen the text embedding. We completely decouple the enhancer from the text-to-image model, which is extremely easy to implement and exhibit better interpretability.

### A.3. Comparison with Distillation-based Methods

The most related works to ours are Guidance Distillation (Meng et al., 2023) and Plug-and-Play (Hsiao et al., 2024), which also aim at reducing the sampling overhead of CFG through distillation. In Figure 12, we provide an illustrative comparison between them and our method. Guidance Distillation takes guidance scale as an additional model entry and processes it in the way similar to the timestamp. The whole parameters of the text-to-image model are fine-tuned under CFG-based supervision. Plug-and-Play trains a guide model in a similar way, where the guide model interacts with the intermediate features of the text-to-image model as in ControlNet (Zhang et al., 2023). Our method, instead, completely decouples the enhancer from the text-to-image model by only modifying the text embedding, which is essentially the model condition. Despite a small number of trainable parameters, our method achieves comparable performance with Guidance Distillation as verified in Section 4.2. This decoupling further enhances the interpretability of our method from both theoretical and empirical perspectives.

### A.4. Comparison with Reward-based Methods

Aiming at further enhancing the image quality given by guided sampling, previous works have proposed to fine-tune the text encoder through reinforcement learning (Chen et al., 2025) and reward propagation (Li et al., 2024a). In Figure 13, we

provide a qualitative comparison between our method and these reward-based methods, i.e., TexForce (Chen et al., 2025) and TextCraftor (Li et al., 2024a). Though these reward-based methods improve the sample quality of guided sampling, their obtained text embeddings are not applicable to unguided sampling. We re-train TexForce for unguided sampling but only observe minor improvement. Therefore, the mechanism of our method, as illustrated in Section 4.3, is different from that of reward-based methods, which we hypothesize is due to the direct CFG-based supervision instead of reward models.

### A.5. Additional Ablation Studies

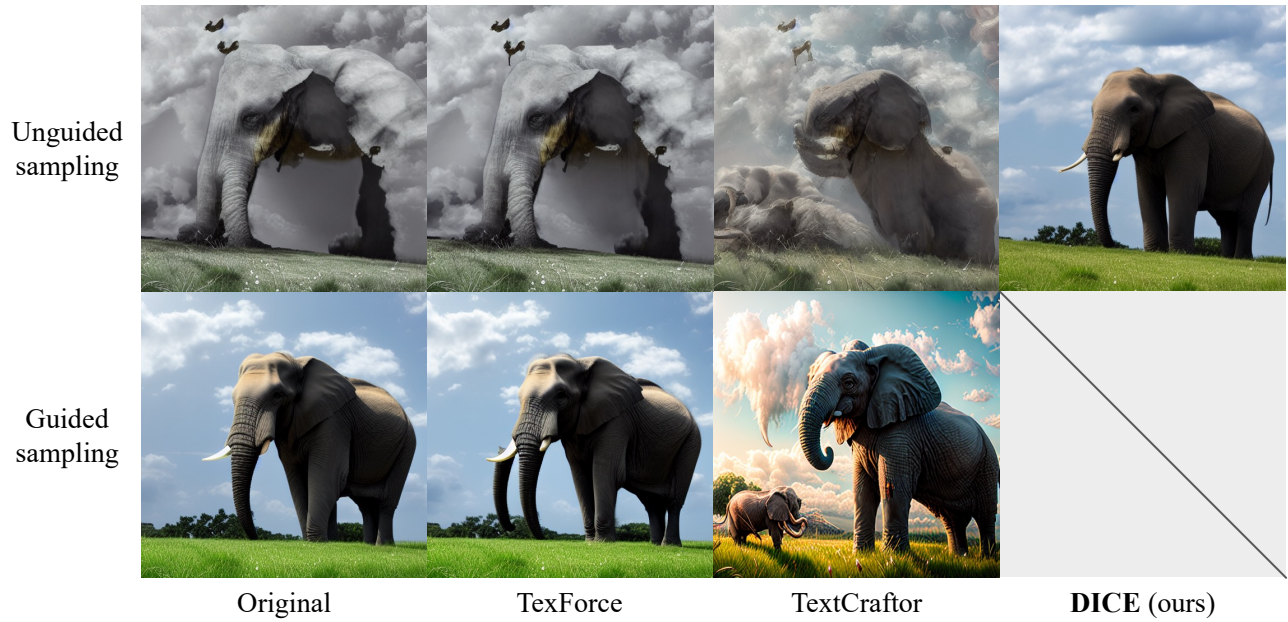
**Enhancer strength.** We take an ablation study on enhancer strength  $\alpha$  which is fixed to 1 during training. The quantitative and qualitative results are shown in Figure 14 and Figure 15. As  $\alpha$  increases in a certain range, the sample quality improves with richer detail and stronger contrast. The enhancer manages to find robust directions that are capable of strengthening the overall image quality while maintaining the semantic information.

**Training iterations.** In Figure 16, we show the performance of our method with respect to FID, CS and AS evolving with training iterations. Our method enjoys a fast convergence.

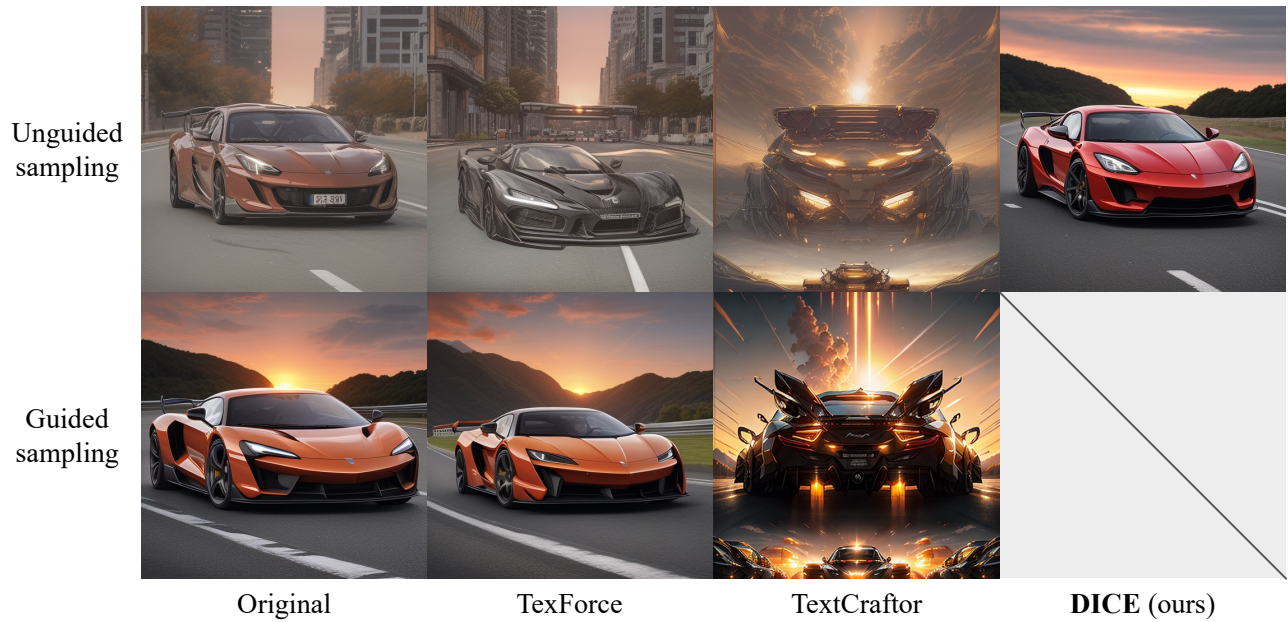
**Combined with guided sampling.** Our method is able to be combined with guided sampling as shown in Figure 17. Combined with guided sampling, our method rapidly improves the image contrast as guidance scale increases.

**NFE budgets.** In Figure 18 and Figure 19, we provide qualitative results as a supplement to Figure 5 on all the text-to-image models involved in this paper, demonstrating the advantage of our method under low NFE budgets.

**Sampling trajectory.** Figure 20 exhibits full sampling trajectories with the corresponding cross-attention maps. The cross-attention maps of DICE differ from the original sampling in terms of the constantly changing background, meaning that our enhanced text embeddings put more attention on the overall image details instead of only the main concepts.



(a) Model: Stable Diffusion v1.5 (Rombach et al., 2022). Text prompt: “an elephant on the grassland, cloud, high quality, realistic”.



(b) Model: DreamShaper. Text prompt: “a supercar on the road, sunset, high quality”.

Figure 13: Comparison with reward-based methods, i.e., TexForce (Chen et al., 2025) and TextCrafter (Li et al., 2024a). The text embeddings obtained by reward-based methods are not applicable to unguided sampling.

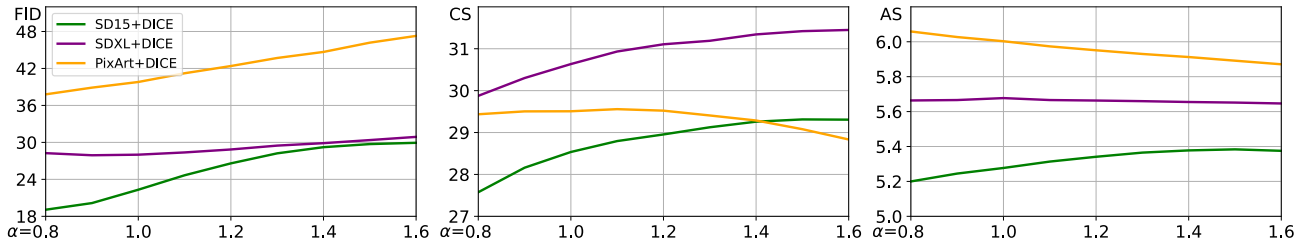


Figure 14: Quantitative results on enhancer strength  $\alpha$ .

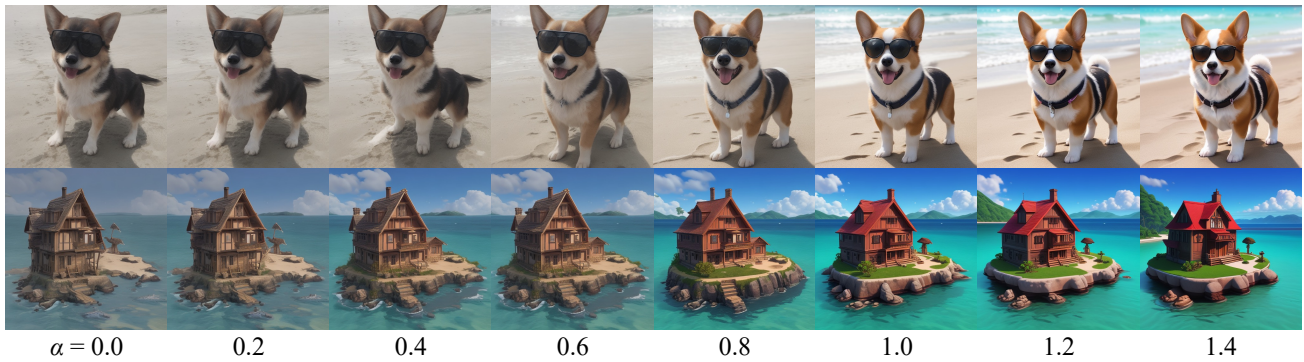


Figure 15: Qualitative results on enhancer strength  $\alpha$ . The enhanced text embeddings exhibit strong semantic consistency. Top: DreamShaper with text prompt “A Corgi wearing sunglasses on the beach”. Bottom: 3D Animation Diffusion with text prompt “A house on an island surrounded by sea, 3D style, best detail, high quality, aesthetic”.

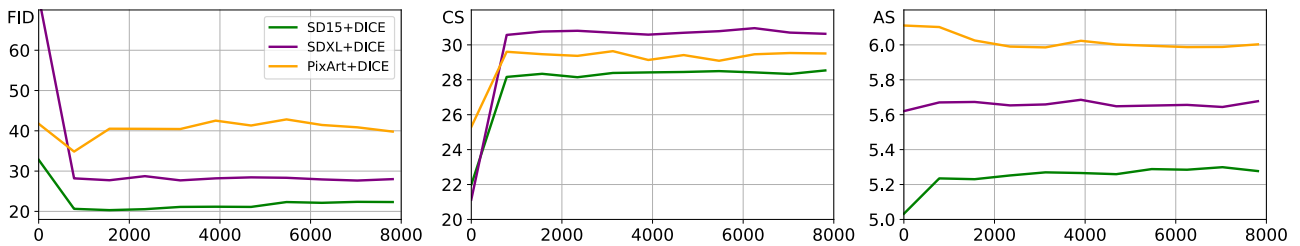
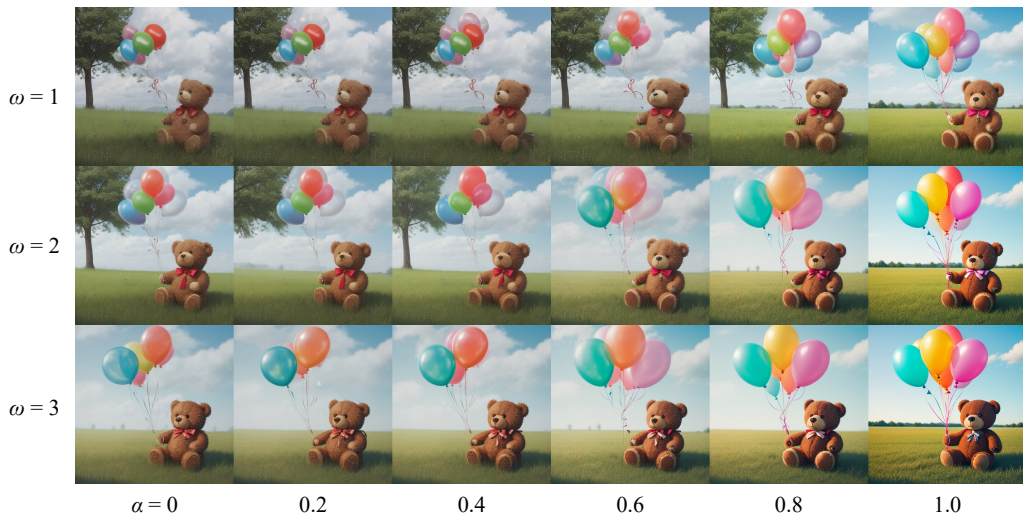


Figure 16: Quantitative results on the training iterations of our method.

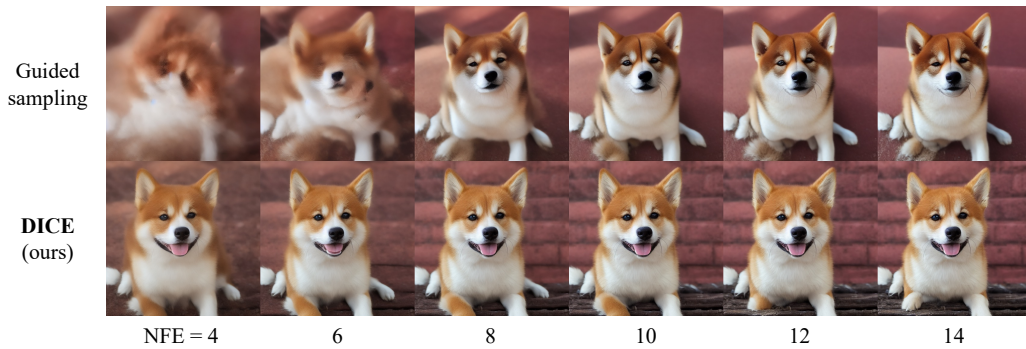


(a) Model: DreamShaper. Text prompt: “photo portrait of a girl”.



(b) Model: DreamShaper. Text prompt: “a teddy bear on the grass with balloons”.

Figure 17: Additional results on enhancer strength  $\alpha$  and guidance scale  $\omega$ . Our enhanced text embeddings can also be combined with guided sampling (i.e.,  $\omega > 1$ ) to improve the overall image quality.



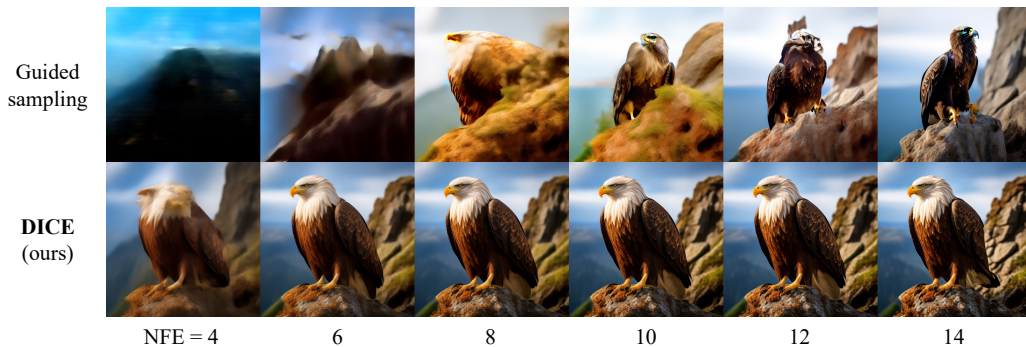
(a) Model: Stable Diffusion v1.5 (Rombach et al., 2022). Text prompt: “close-up photo of a cute smiling shiba inu”.



(b) Model: DreamShaper. Text prompt: “flowers on the table”.

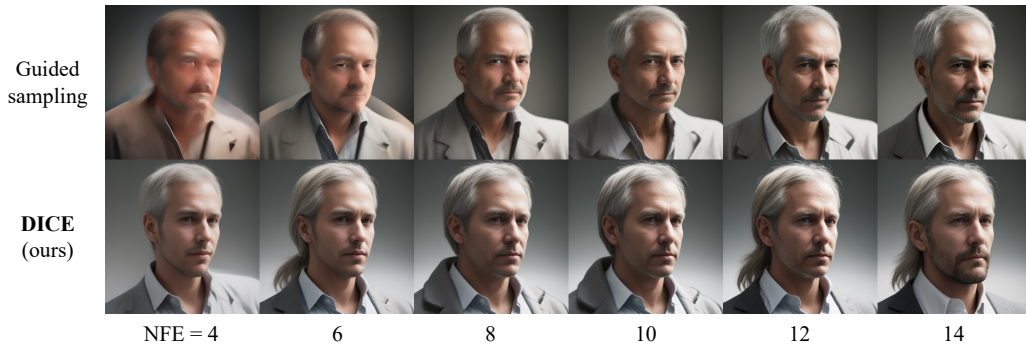


(c) Model: Stable Diffusion XL (Podell et al., 2024). Text prompt: “a robot in the city, perfect detail, 8k, best quality”.

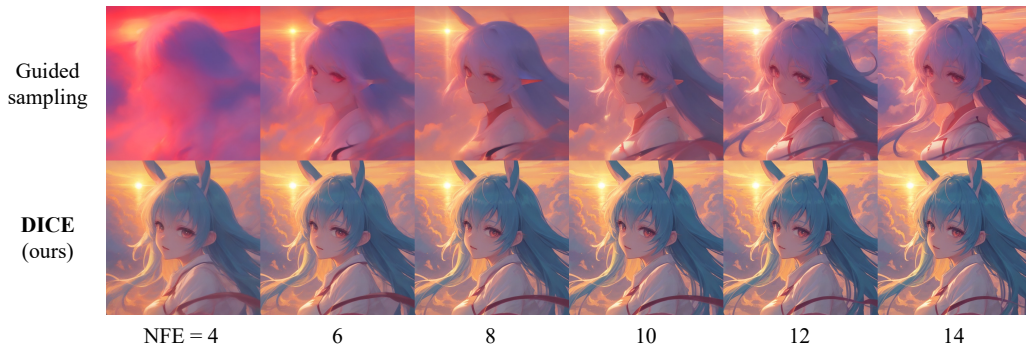


(d) Model: Pixart- $\alpha$  (Chen et al., 2024b). Text prompt: “close-up photo of an eagle on the cliff”.

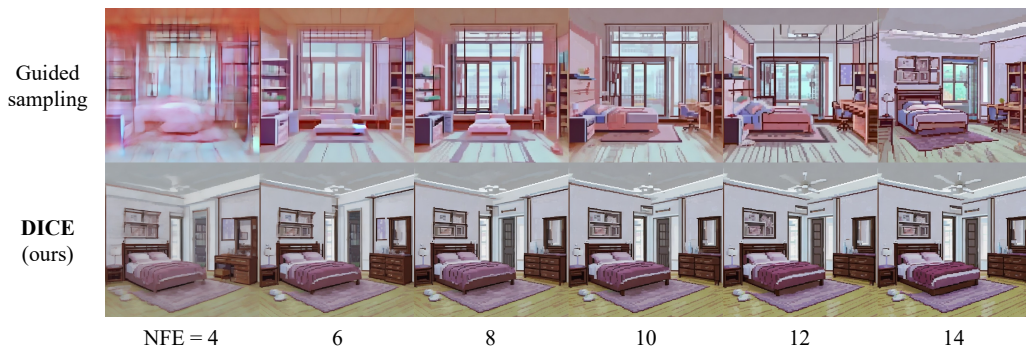
Figure 18: Qualitative results under different NFEs. Guidance scale of 5 is used for all guided sampling.



(a) Model: AbsoluteReality. Text prompt: “photo portrait of a man”.



(b) Model: Anime Pastel Dream. Text prompt: “an anime character on the cloud, sunset, close-up”.

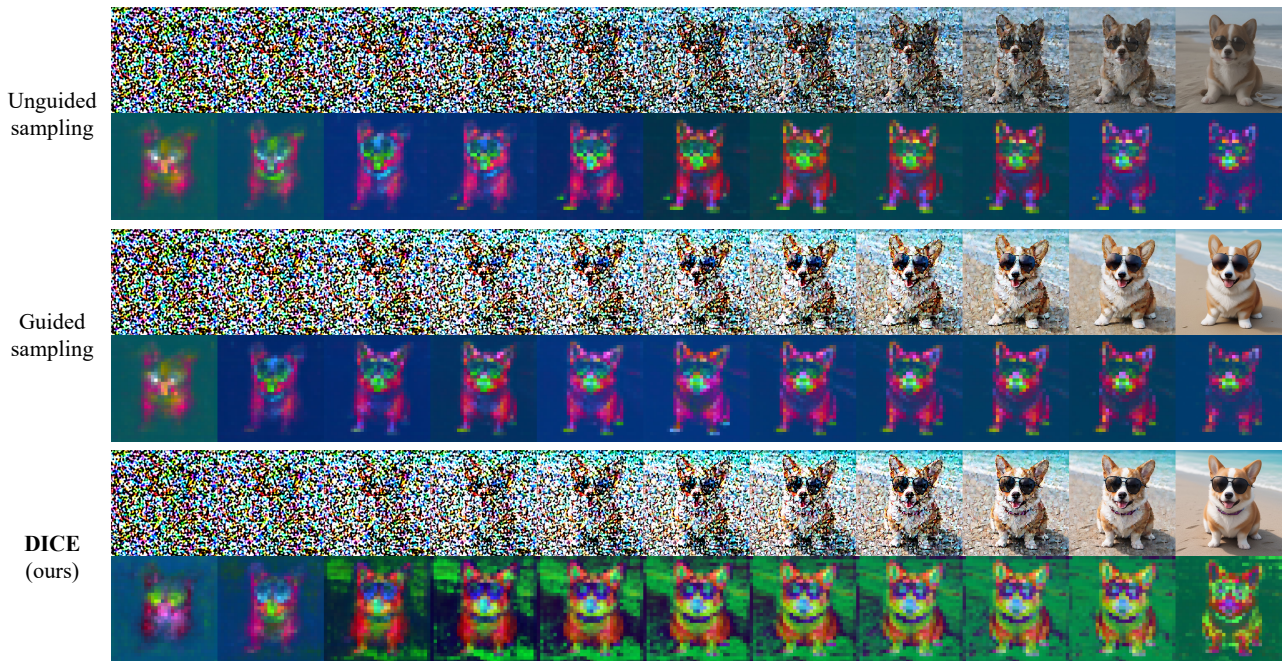


(c) Model: DreamShaper PixelArt. Text prompt: “a clean bedroom, pixel art”.

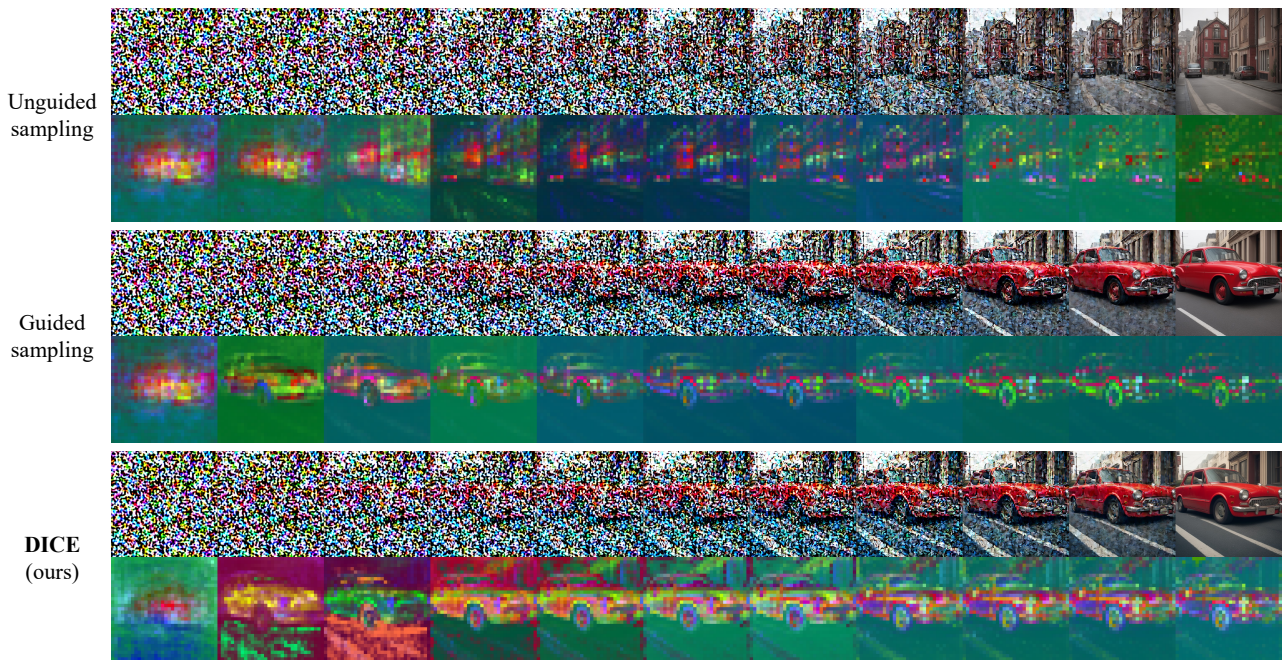


(d) Model: 3D Animation Diffusion. Text prompt: “a cute princess, cartoon, best quality”.

Figure 19: Qualitative results under different NFEs for other Stable Diffusion variants.



(a) Model: DreamShaper (Lykon, 2023). Text prompt: “a Corgi wearing sunglasses on the beach”.



(b) Model: DreamShaper (Lykon, 2023). Text prompt: “a red car by the street”.

Figure 20: Qualitative results on sampling trajectory and cross-attention maps from  $t = T$  to  $t = 0$ . Images are generated by 10-step DPM-Solver++ (Lu et al., 2022) with the same random seed in each subfigure.